LETTER

doi:10.1038/nature24679

Synchrotron scanning reveals amphibious ecomorphology in a new clade of bird-like dinosaurs

Andrea Cau[1], Vincent Beyrand[2,3], Dennis F. A. E. Voeten[2,3], Vincent Fernandez[2], Paul Tafforeau[2], Koen Stein[4], Rinchen Barsbold[5], Khishigjav Tsogtbaatar[6], Philip J. Currie[7] & Pascal Godefroit[8]

Maniraptora includes birds and their closest relatives among theropod dinosaurs[1–5]. During the Cretaceous period, several maniraptoran lineages diverged from the ancestral coelurosaurian *bauplan* and evolved novel ecomorphologies, including active flight[2], gigantism[3], cursoriality[4] and herbivory[5]. Propagation X-ray phase-contrast synchrotron microtomography of a well-preserved maniraptoran from Mongolia, still partially embedded in the rock matrix, revealed a mosaic of features, most of them absent among non-avian maniraptorans but shared by reptilian and avian groups with aquatic or semiaquatic ecologies[6–14]. This new theropod, *Halszkaraptor escuilliei* gen. et sp. nov., is related to other enigmatic Late Cretaceous maniraptorans from Mongolia[15,16] in a novel clade at the root of Dromaeosauridae[17]. This lineage adds an amphibious ecomorphology to those evolved by maniraptorans: it acquired a predatory mode that relied mainly on neck hyperelongation for food procurement, it coupled the obligatory bipedalism of theropods with forelimb proportions that may support a swimming function, and it developed postural adaptations convergent with short-tailed birds.

Theropoda Marsh, 1881
Maniraptora Gauthier, 1986
Dromaeosauridae Matthew and Brown, 1922
Halszkaraptorinae subfam. nov.

Definition. The most inclusive clade that contains *Halszkaraptor escuilliei* gen. et sp. nov., but not *Dromaeosaurus albertensis*, *Unenlagia comahuensis*, *Saurornithoides mongoliensis* or *Vultur gryphus*. Taxa included: *Halszkaraptor escuilliei*, *Hulsanpes perlei*[15] and *Mahakala omnogovae*[16]. Type species: *Halszkaraptor escuilliei*.

Diagnosis. Long-necked dromaeosaurids with proximal caudal vertebrae that have horizontally oriented zygapophyses and prominent zygodiapophyseal laminae; flattened ulna with a sharp posterior margin; metacarpal III shaft transversely as thick as that of metacarpal II; ilium with a shelf-like supratrochanteric process; posterodistal surface of femoral shaft with an elongate fossa bound by a lateral crest; proximal half of metatarsal III unconstricted and markedly convex anteriorly.

Halszkaraptor escuilliei gen. et sp. nov.

Etymology. *Halszka*, a Latinized form of archaic Polish *Halżka*, honours Halszka Osmólska (1930–2008) for her contributions to theropod palaeontology, which include the description of the first halszkaraptorine species found (*Hulsanpes perlei*)[15]; *raptor*, 'robber' (Latin). The specific name *escuilliei* refers to François Escuillié, who returned the poached holotype to Mongolia.

Holotype. MPC (Institute of Paleontology and Geology, Mongolian Academy of Sciences, Ulaanbaatar, Mongolia) D-102/109 (Figs 1, 2, 3a–f, Extended Data Figs 2–8, Supplementary Table 1); an articulated and almost complete skeleton preserved three-dimensionally.

Locality and horizon. Bayn Dzak Member, Djadokhta Formation (Campanian, ~75–71 Mya), Ukhaa Tolgod, Mongolia (see Supplementary Information).

Diagnosis. Autapomorphies are marked by asterisks; differential diagnosis can be found in Supplementary Information. Platyrostral premaxilla that forms 32% of snout length* and bears 11 teeth*; external naris posterior to the premaxillary oral margin; rod-like jugal with an ascending process excluded from the orbital margin that forms only 10% of the postorbital bar*; rod-like ventral ramus of the postorbital; 22 presacral vertebrae; neck forms 50% of snout–sacrum length*; absence of epipophyses*; ridge-like cervical neural spines restricted to the 2nd–5th vertebrae*; postzygapophyses on cervicals 2–5 are fused medially and form single lobate processes*; pleurocoels restricted to cervicals 7–9; tuber-like neural spines in tail are restricted to the 1st–3rd vertebrae*; proximal-most chevrons large and pentagonal*; transition point in 7th–8th caudals; 3rd finger longer than 2nd; elongate pedal phalanx III-1 is 47% of the length of metatarsal III*.

We performed multi-resolution scanning at the European Synchrotron Radiation Facility using BM05 and ID19 beamlines; this revealed all the elements that were still embedded in matrix and demonstrated the integrity of the specimen (Supplementary Information, Extended Data Figs 1–3). Histological analysis indicates that MPCD-102/109 was a subadult individual (Supplementary Information, Extended Data Figs 4, 5). The platyrostral premaxilla with a dorsolaterally oriented external naris that is retracted beyond the oral margin is unique among theropods, although in its elongation, the premaxilla is similar to those of spinosaurids[8] (Fig. 2a–g, Extended Data Figs 6, 8). A hypertrophied network of neurovascular chambers penetrates throughout the premaxilla. This condition is also seen in aquatic reptiles, such as plesiosaurs[12] and crocodiles (Fig. 2e, f, Extended Data Fig. 8), whereas in other theropods this neurovascular network resides exclusively in the lateral half of the premaxilla[13]. Each premaxilla bears 11 teeth (Fig. 2g, Extended Data Figs 6, 7), which is the highest number found in any dinosaur. Spinosaurids and *Pelecanimimus* approach *Halszkaraptor* in having six or seven premaxillary teeth[8], whereas most theropods have four. Both the maxilla and the dentary bear 20–25 teeth; this is comparable to the condition seen in unenlagiines[17] and baryonychines[8]. Although some maniraptoriforms carry a total of over 30 small maxillary and/or dentary teeth[5], most theropods have fewer than 20. The heterodont dentition of *Halszkaraptor* involves closely packed premaxillary teeth with long roots and incisiviform crowns, and a labiolingually compressed posterior dentition with shorter roots and concave distal crown margins (Fig. 3d, Extended Data Fig. 7). All teeth lack serrations, as is the case in most paravians[7], spinosaurines[8] and a few other theropods. Synchrotron scanning revealed a delayed replacement pattern in the anterior dentition[14], whereas the majority of the posterior teeth are associated with a replacement tooth.

[1]Geological and Palaeontological Museum 'Giovanni Capellini', I-40126 Bologna, Italy. [2]European Synchrotron Radiation Facility, F-38043 Grenoble, France. [3]Department of Zoology and Laboratory of Ornithology, Palacký University, CS-40220 Olomouc, Czech Republic. [4]Earth System Science – AMGC Vrije Universiteit Brussel, B-1050 Brussels, Belgium. [5]Palaeontological Center, Mongolian Academy of Sciences, Ulaanbaatar 201-351, Mongolia. [6]Institute of Palaeontology and Geology, Mongolian Academy of Sciences, Ulaanbaatar 210-351, Mongolia. [7]Department of Biological Sciences, University of Alberta, Edmonton, Alberta T6G 2E9, Canada. [8]Directorate Earth & History of Life, Royal Belgian Institute of Natural Sciences, B-1000 Brussels, Belgium.

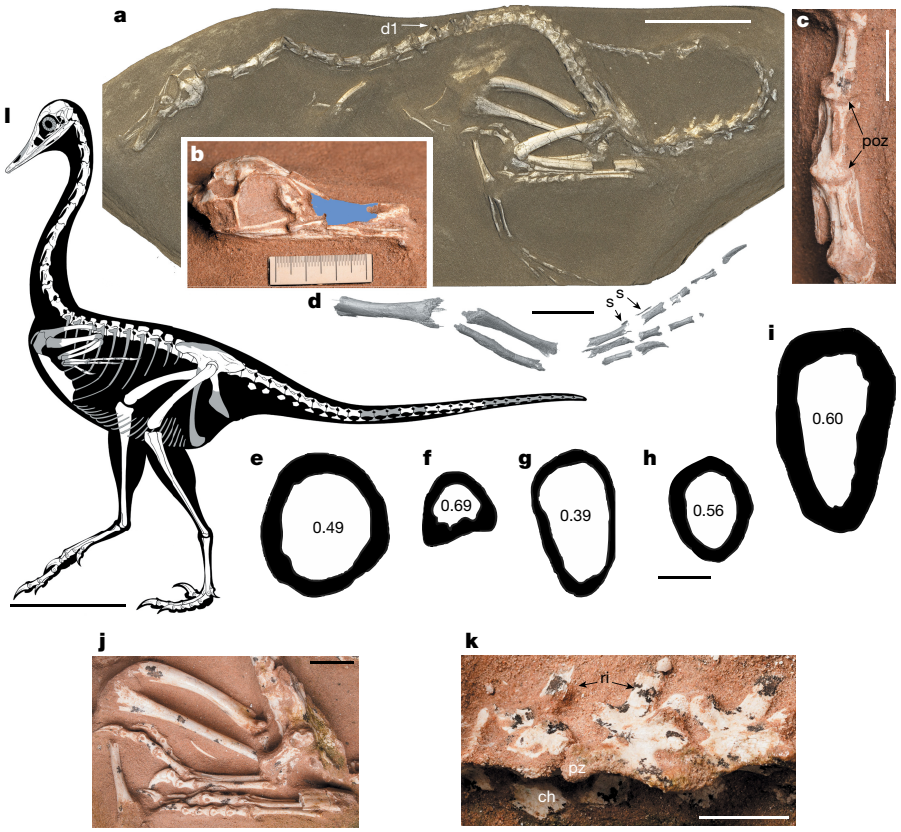

Figure 1 | *H. escuilliei* MPC D-102/109. a, 3D rendering of synchrotron data that provides an overview of the exposed skeleton with plaster-restored parts removed. d1, first dorsal vertebra. **b**, Exposed skull in lateral view with restored elements in blue. **c**, Cervical vertebrae 2–4 in dorsal view. Poz, postzygapophysis. **d**, 3D rendering of left forelimb. Note splints of bone (marked as 's') near metacarpal III and adjacent phalanx that are still embedded in the main slab (Supplementary Information). **e**–**i**, Virtual cross-sections of right humerus mid-shaft (**e**), right radius mid-shaft (**f**), proximal end of right ulna (**g**), right ulna mid-shaft (**h**) and left tibia mid-shaft (**i**). All are oriented with their lateral margin at the bottom. **j**, Exposed pelvis and hindlimbs. **k**, Proximal caudal vertebrae in dorsal view. ch, chevron; pz, prezygapophysis; ri, rib. **l**, Skeletal reconstruction with missing elements in grey. Numbers in **e**–**i** indicate cortical/cross-sectional area ratios. Scale bars, 70 mm (**a**), 30 mm (**b**), 20 mm (**c**, **d**, **j**, **k**), 2 mm (**e**–**i**) and 100 mm (**l**).

Compared to body size, the neck is elongate and forms 50% of the snout–sacrum length; this is the highest value found among Mesozoic paravians[18,19] thus far. Cervical centra 2 to 10 are low, elongate and transversely compressed towards their ventral edges (Figs 1a, 1c, 3e). Cervical neural spines are poorly developed and remain limited to the first five vertebrae (Fig. 1c). The first five neural arches are also unique among theropods in their lack of inter-postzygapophyseal spaces: instead, each pair of postzygapophyses forms a single planar surface that faces ventrally and has a convex posterior margin. This morphology is also seen in some long-necked chelonians[7] and a few birds (for example, *Cygnus*, Fig. 3h–j). No epipophyses are present and pneumatic recesses are present only in the 7th–9th cervical centra. The diapophyses are positioned at the anterolateral corners of all vertebrae, at the bases of the prezygapophyses. The robust cervical ribs are fused to both the parapophyses and the diapophyses, as is the case in *Mahakala*[16]. The proximal tail vertebrae (Fig. 1k) share with those of *Mahakala* the combination of elongate centra, wide and horizontally oriented zygapophyses, and prominent zygodiapophyseal laminae that form lateral shelves[16]. The caudal neural spines are reduced, tuber-like and restricted to the first three vertebrae. The proximal chevrons are pentagonal and plate-like. The large sternal plates are unfused medially.

In the exposed forelimb bones, cortical thickness decreases towards the epiphyseal ends and culminates in extremities that are almost completely dissolved (Fig. 1d). This preservation pattern is also seen in *Mahakala*[16]. The whole ulna is flattened and possesses an acute posterior margin (Fig. 1g–h), traits that are also similar to *Mahakala*, but which differ from other paravians[16,17]. The hand differs from non-scansoriopterygid theropods[20] in the progressive elongation of the lateral fingers, with the third being the longest and most robust (Figs 1d, 3e). In the ilium, the iliofibularis muscle origin is hypertrophied and shelf-like, as is the case in *Mahakala*[16]. The 76-mm-long femur has a large trochanteric crest, a tuber-like 4th trochanter and an elongate posterolateral ridge that distally bounds an elongate ansa iliofibularis; the last feature is shared exclusively with *Mahakala*[16]. The metatarsus lacks cursorial adaptations and measures 80% of femoral length; in the comparably sized *Mahakala*, the metatarsus is longer than the femur[16]. The distal ends of metatarsals II and III are ginglymoidal (Fig. 3e), as is the case in many dromaeosaurids[15–17,21,22]. As is the condition in the other halszkaraptorines and in many basal avialans[22], the proximal half of metatarsal III is not constricted and dorsally convex. The distal shaft of metatarsal III differs from those of *Hulsanpes* and *Mahakala* in that it does not overlap metatarsal II and lacks a distinct transverse constriction proximal to the trochlea[15,16]. The distal end of the first toe reaches the level of the articular facet of the second ungual. The phalanges of the second-to-fourth toes shorten toward the distal ends of the toes. The second toe is half the length of the third (Fig. 3e), with a stout phalanx II-2 and a large falciform ungual, similar to those in other paravians[17,21,22]. Phalanx III-1 is slender and elongate (47% of the length of metatarsal III). The third and fourth unguals are only slightly recurved.

Phylogenetic analyses place *Halszkaraptor* within a new and basal clade of dromaeosaurids here described as Halszkaraptorinae, which also includes the hitherto enigmatic *Hulsanpes* and *Mahakala* (Fig 3a–f, Extended Data Figs 9, 10, Supplementary Information). The unusual morphology of *Halszkaraptor* suggests a semiaquatic ecology. Piscivory,

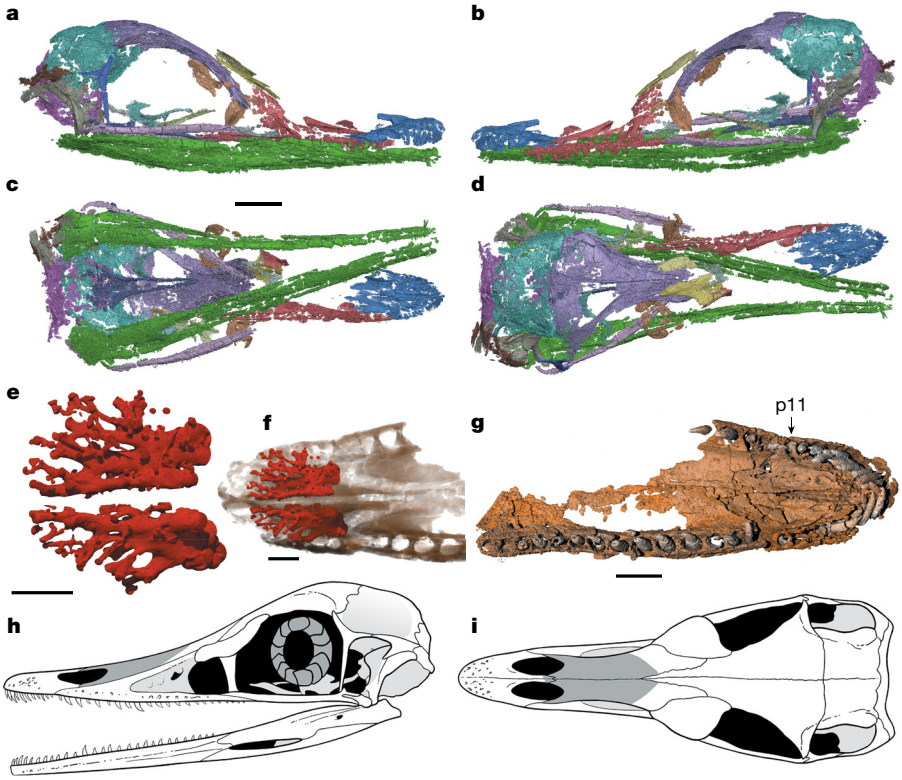

Figure 2 | Skull of *H. escuilliei* MPC D-102/109. a–d, 3D visualization of skull in right lateral (**a**), left lateral (**b**), ventral (**c**) and dorsal (**d**) views. **e**, **f**, Synchrotron scan segmentation of the snout in dorsal view (**f**) that shows the enlarged bony chambers (**e**) that house the blood vessels and the rostral terminations of the maxillary branch of the trigeminal nerves. **g**, 3D rendering of preantorbital part of skull in palatal view. p11, 11th premaxillary tooth. **h**, **i**, Skeletal reconstruction of skull in lateral (**h**) and dorsal (**i**) views. Scale bars, 9 mm (**a–d**) and 3 mm (**e–g**).

documented among basal dromaeosaurids[23,24], is inferred from several features of *Halszkaraptor*, including a platyrostral premaxilla[8], narial retraction[8], an extensively developed neurovascular plexus in the premaxilla[12], an increase in the number of teeth[8], and a pattern of protracted replacement in anterior dentition[14], all of which are shared by aquatic predators. Neck elongation is widespread among sauropsids that use an ambush mode of predation in water[6], and the cervical morphology of *Halszkaraptor* (unique among non-avian theropods) is exclusively shared with semiaquatic lineages such as araripemydid turtles[7] and some long-necked anatids (Fig. 3g–i). The horizontally oriented zygapophyses in the neck and tail vertebrae of halszkaraptorines would have permitted the axial undulatory swimming mode that is typical of taxa with axially elongated body shapes[6]. The unusual forelimb morphology is not inconsistent with a semiaquatic ecology. Although the fragmentary preservation of the pectoral region prevents a detailed reconstruction of forelimb range of motion, on the basis of phylogenetic bracketing[17,26] we infer that the glenoid in *Halszkaraptor* faces laterally, as it does in forelimb-assisted swimming tetrapods[25]. The upper limb exhibits flattening of the long bones, which resulted in a forearm and distal humerus that possess ellipsoid cross-sections (Fig. 1e–h). This condition is widespread among secondarily aquatic amniotes[9–11]. Morphometric comparison of the forelimb of *Halszkaraptor* with those of terrestrial, aquatic and flying sauropsids supports the idea that this theropod possessed swimming adaptations (Fig. 4, Supplementary Information). Among the disparate locomotory morphologies of birds, the forelimb of *Halszkaraptor* clusters with those of wing-propelled swimming birds, with parameters intermediate between those of penguins and those of other aquatic birds (Fig. 4b). The asymmetrical digital elongation in *Halszkaraptor* exceeds known maniraptoran conditions and differs from the extreme proportions of scansoriopterygids, which have been interpreted as gliding adaptations[20]; instead, the proportions of *Halszkaraptor* cluster with those of long-necked aquatic reptiles (Fig. 4a).

Halszkaraptor is interpreted as an amphibious theropod: an obligatory biped on land and a swimmer that used its forelimbs to manoeuvre in water and that relied on its long neck for foraging. The hyper-elongate neck of *Halszkaraptor*, countered by a less-elongated tail, suggests that its centre of mass was shifted anterior to the hip region. Although the forward centre-of-mass position is functionally adaptive during swimming[27], it challenges the obligate bipedal posture of theropods that requires the centre of mass to be near the hip joint[28]. During their evolution, short-tailed birds have compensated for a similar anterior shift of their centres of mass by increasing hip extension ability[28]. The shelf-like supratrochanteric process of the ilium and the posterolateral fossa–crest complex in the femur, which are synapomorphies of halszkaraptorines[16], indicate an increased hip extension moment arm for the iliofibularis muscle[28]; this would have supported a body posture that was more erect on land, which is analogous to the postures of modern birds.

The ecomorphology of the Halszkaraptorinae markedly deviates from those of other maniraptorans and may represent the first case among non-avian dinosaurs of a double locomotory module[29] that includes forelimb-assisted swimming. It illustrates how much of the diversity of Dinosauria remains undiscovered, even in intensely studied regions such as Mongolia.

Data Availability This published work and the nomenclatural acts it contains have been registered in ZooBank. The ZooBank life science identifiers can be resolved and the associated information viewed by appending the life science identifiers to the prefix http://zoobank.org/. The life science identifier for this publication is LSID urn:lsid:zoobank.org:pub:7FE47556-61CD-4A25-AAD6-A469DA664480; for Halszkaraptorinae, LSID urn:lsid:zoobank.org:act:12E4325C-D1DA-4EAF-8539-25C90B028B7C; for *Halszkaraptor*, LSID urn:lsid:zoobank.org:act:B14CF603-F0E9-4DC6-9BB1-D215549B6D4F; and for *H. escuilliei*, LSID urn:lsid:zoobank.org:act:6C4BFD0B-DAF7-4B94-B97E-6F9423EB6D35. The phylogenetic and morphometric data supporting the findings of this study are available within the paper and its Supplementary Information. The synchrotron data used in this study are available on the ESRF open access database at http://paleo.esrf.fr.

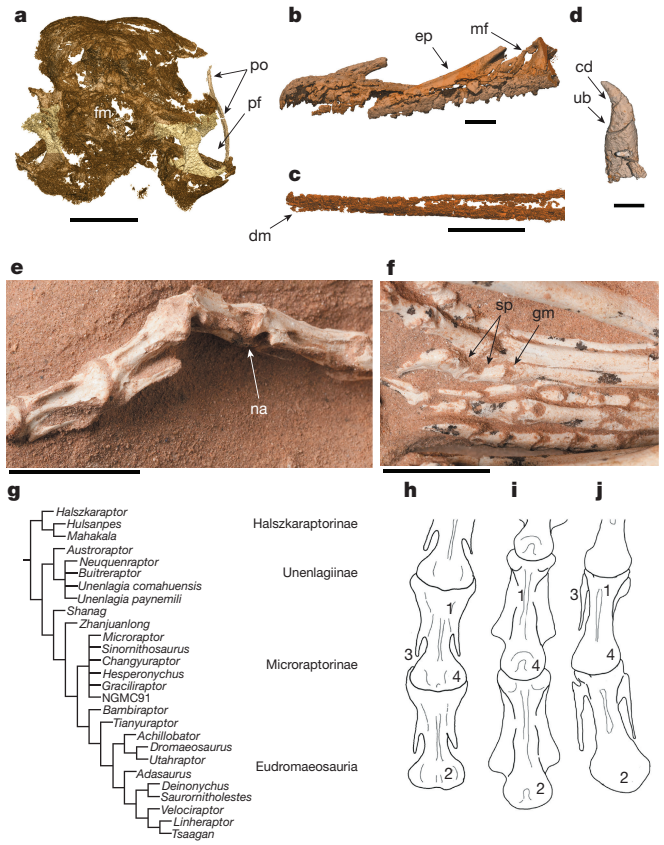

Figure 3 | *H. escuilliei* phylogenetic affinities and comparisons for its unique postcranial features. a–**e**, Dromaeosaurid synapomorphies in *Halszkaraptor*. **a**, Skull in occipital view. fm, foramen magnum; po, postorbital; pf, enlarged paraquadrate fenestra. **b**, Premaxilla and maxilla in lateral view. ep, elongate pre-antorbital part of maxilla; mf, dorsally placed maxillary fenestra. **c**, Mandible in lateral view. dm, dentary ventral and dorsal margins subparallel. **d**, Dentary tooth in lingual view. cd, concave distal margin of crown; ub, unconstricted crown base. **e**, Neck in ventrolateral view. na, neural arch extended to level of intercentral facet. **f**, Feet in extensor view. gm, ginglymoidal distal end of metatarsal II; sp, short and stout phalanges of second toe. **g**, Phylogenetic position of *Halszkaraptor* among Maniraptora, on the basis of parsimony analysis using TNT software[30] on two independently developed datasets[22] (for complete topologies and tree statistics, see Supplementary Information). **h**–**j**, Dorsal view of anterior cervical vertebrae of *Cygnus* (**h**), the fresh-water chelonian *Araripemys*[7] (**i**) and *Halszkaraptor* (**j**). These vertebrae share a combination of features: (1) elongate neural arches with reduced ridge-like neural spines; (2) merged postzygapophyses that form a lobate process; (3) ribs fused to vertebra; and (4) horizontally oriented zygapophyseal facets. Scale bars, 9 mm (**a**, **c**), 3 mm (**b**); 1 mm (**d**) and 30 mm (**e**, **f**).

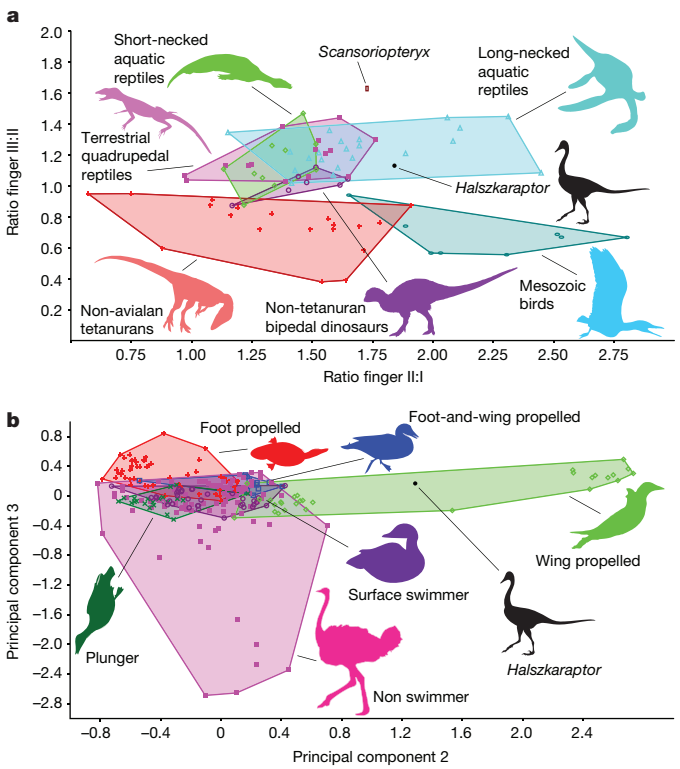

Figure 4 | Morphometric analyses of aquatic adaptations in the *Halszkaraptor* forelimb. a, Binary plot of length ratios among manual digits I–III in aquatic and terrestrial sauropsids ($n = 84$): *Halszkaraptor* clusters with long-necked aquatic reptiles. **b**, Binary plot of principal components 2 and 3 from a morphometric analysis of ten skeletal characters of the forelimb and sternum in birds ($n = 246$; principal component 1 describes body size variation and is therefore not considered; see Supplementary Information): *Halszkaraptor* clusters with wing-propelled swimming birds. Silhouettes in **a** provided by D. Bonadonna and L. Panzarin.

Online Content Methods, along with any additional Extended Data display items and Source Data, are available in the online version of the paper; references unique to these sections appear only in the online paper.

Received 21 August; accepted 1 November 2017.
Published online 6 December 2017.

1. Gauthier, J. Saurischian monophyly and the origin of birds. *Memoirs Cal. Acad. Sci.* **8,** 1–55 (1986).
2. Witmer, L. M. in *Mesozoic Birds: Above the Heads of Dinosaurs* (eds Chiappe, L. M. & Witmer, L. M.) 3–30 (Univ. California Press, 2002).
3. Xu, X., Tan, Q., Wang, J., Zhao, X. & Tan, L. A gigantic bird-like dinosaur from the Late Cretaceous of China. *Nature* **447,** 844–847 (2007).
4. Holtz, T. R. Jr. The arctometatarsalian pes, an unusual structure of the metatarsus of Cretaceous Theropoda (Dinosauria: Saurischia). *J. Vertebr. Paleontol.* **14,** 480–519 (1995).
5. Zanno, L. E. & Makovicky, P. J. Herbivorous ecomorphology and specialization patterns in theropod dinosaur evolution. *Proc. Natl Acad. Sci. USA* **108,** 232–237 (2011).
6. Massare, J. A. Swimming capabilities of Mesozoic marine reptiles: implications for method of predation. *Paleobiology* **14,** 187–205 (1988).
7. Meylan, P. A. Skeletal morphology and relationships of the early Cretaceous side-necked turtle, *Araripemys barretoi* (Testudines: Pelomedusoides: Araripemydidae), from the Santana Formation of Brazil. *J. Vertebr. Paleontol.* **16,** 20–33 (1996).
8. Charig, A. J. & Milner, A. C. *Baryonyx walkeri*, a fish-eating dinosaur from the Wealden of Surrey. *Bull. Nat. Hist. Mus. Lond. (Geol.)* **53,** 11–70 (1997).
9. Caldwell, M. W. From fins to limbs to fins: limb evolution in fossil marine reptiles. *Am. J. Med. Genet.* **112,** 236–249 (2002).
10. Thewissen, J. G. M. & Taylor, M. A. in *Fins into Limbs: Evolution, Development, and Transformation* (ed. Hall, B. K.) 310–322 (Univ. Chicago Press, 2007).
11. Habib, M. The structural mechanics and evolution of aquaflying birds. *Biol. J. Linn. Soc.* **99,** 687–698 (2010).
12. Foffa, D., Sassoon, J., Cuff, A. R., Mavrogordato, M. N. & Benton, M. J. Complex rostral neurovascular system in a giant pliosaur. *Naturwissenschaften* **101,** 453–456 (2014).
13. Barker, C. T., Naish, D., Newham, E., Katsamenis, O. L. & Dyke, G. Complex neuroanatomy in the rostrum of the Isle of Wight theropod *Neovenator salerii*. *Sci. Rep.* **7,** 3749 (2017).
14. Kear, B. P., Larsson, D., Lindgren, J. & Kundrát, M. Exceptionally prolonged tooth formation in elasmosaurid plesiosaurians. *PLoS ONE* **12,** e0172759 (2017).
15. Osmólska, H. *Hulsanpes perlei* n.g. n.sp. (Deinonychosauria, Saurischia, Dinosauria) from the Upper Cretaceous Barun Goyot Formation of Mongolia. *Neues Jahrb. Geol. Paläontol. Monat.* **7,** 440–448 (1982).
16. Turner, A. H., Pol, D. & Norell, M. A. Anatomy of *Mahakala omnogovae* (Theropoda: Dromaeosauridae), Tögrögiin Shiree, Mongolia. *Am. Mus. Nov.* **3722,** 1–66 (2011).
17. Turner, A. H., Makovicky, P. J. & Norell, M. A. A review of dromaeosaurid systematics and paravian phylogeny. *Bull. Am. Mus. Nat. Hist.* **371,** 1–206 (2012).
18. Osmólska, H., Roniewicz, E. & Barsbold, R. A new dinosaur, *Gallimimus bullatus* n. gen., n. sp. (Ornithomimidae) from the Upper Cretaceous of Mongolia. *Palaeontol. Pol.* **27,** 103–143 (1972).
19. Balanoff, A. M. & Norell, M. A. Osteology of *Khaan mckennai* (Oviraptorosauria: Theropoda). *Bull. Am. Mus. Nat. Hist.* **372,** 1–77 (2012).

20. Xu, X. *et al.* A bizarre Jurassic maniraptoran theropod with preserved evidence of membranous wings. *Nature* **521,** 70–73 (2015).
21. Ostrom, J. H. Osteology of *Deinonychus antirrhopus*, an unusual theropod from the Lower Cretaceous of Montana. *Peabody Mus. Nat. Hist. Bull*. **30,** 1–165 (1969).
22. Cau, A., Brougham, T. & Naish, D. The phylogenetic affinities of the bizarre Late Cretaceous Romanian theropod *Balaur bondoc* (Dinosauria, Maniraptora): dromaeosaurid or flightless bird? *PeerJ* **3,** e1032 (2015).
23. Gianechini, F. A., Makovicky, P. J. & Apesteguía, S. The teeth of the unenlagiine theropod *Buitreraptor* from the Cretaceous of Patagonia, Argentina, and the unusual dentition of the Gondwanan dromaeosaurids. *Acta Palaeontol. Pol.* **56,** 279–290 (2011).
24. Xing, L. *et al.* Piscivory in the feathered dinosaur *Microraptor*. *Evolution* **67,** 2441–2445 (2013).
25. Carpenter, K., Sanders, F., Reed, B., Reed, J. & Larson, P. Plesiosaur swimming as interpreted from skeletal analysis and experimental results. *Trans. Kans. Acad. Sci.* **113,** 1–34 (2010).
26. Senter, P. Comparison of forelimb function between *Deinonychus* and *Bambiraptor* (Theropoda: Dromaeosauridae). *J. Vertebr. Paleontol.* **26,** 897–906 (2006).
27. Ribak, G., Weihs, D. & Arad, Z. How do cormorants counter buoyancy during submerged swimming? *J. Exp. Biol.* **207,** 2101–2114 (2004).
28. Hutchinson, J. R. The evolution of femoral osteology and soft tissues on the line to extant birds (Neornithes). *Zool. J. Linn. Soc.* **131,** 169–197 (2001).
29. Gatesy, S. M. & Dial, K. P. Locomotor modules and the evolution of avian flight. *Evolution* **50,** 331–340 (1996).
30. Goloboff, P., Farris, J. S. & Nixon, K. C. TNT, a free program for phylogenetic analysis. *Cladistics* **24,** 774–786 (2008).

Supplementary Information is available in the online version of the paper.

Acknowledgements We thank the European Synchrotron Radiation Facility for granting us beam time at ID19 and BM05 beamlines; Y. Pommery for his work on teeth segmentation; T. Hubin for photographs; A. Halamski and D. Madzia for information on *Hulsanpes* holotype; and M. Auditore for the skeletal reconstructions. U. Lefèvre and L. Van Bossuyt took conventional X-ray pictures at the Veterinary School of Liège University. Silhouettes in Fig. 4a were provided by D. Bonadonna and L. Panzarin and are used with their permission. The program TNT was made available by the sponsorship of the Willi Hennig Society.

Author Contributions A.C. and P.G. designed the project. P.G. supervised the preparation of the specimen. P.T., V.B., D.F.A.E.V. and V.F. performed synchrotron scanning, data processing and segmentation, and created the 2D and 3D renderings. K.S. conducted the histological analysis. R.B., K.T. and P.J.C. provided information on Mongolian theropods and geological setting. A.C. conducted the phylogenetic analyses. A.C. wrote the manuscript with input from all other authors.

Author Information Reprints and permissions information is available at www.nature.com/reprints. The authors declare no competing financial interests. Readers are welcome to comment on the online version of the paper. Publisher's note: Springer Nature remains neutral with regard to jurisdictional claims in published maps and institutional affiliations. Correspondence and requests for materials should be addressed to A.C. (cauand@gmail.com).

Reviewer Information *Nature* thanks T. Holtz Jr and the other anonymous reviewer(s) for their contribution to the peer review of this work.

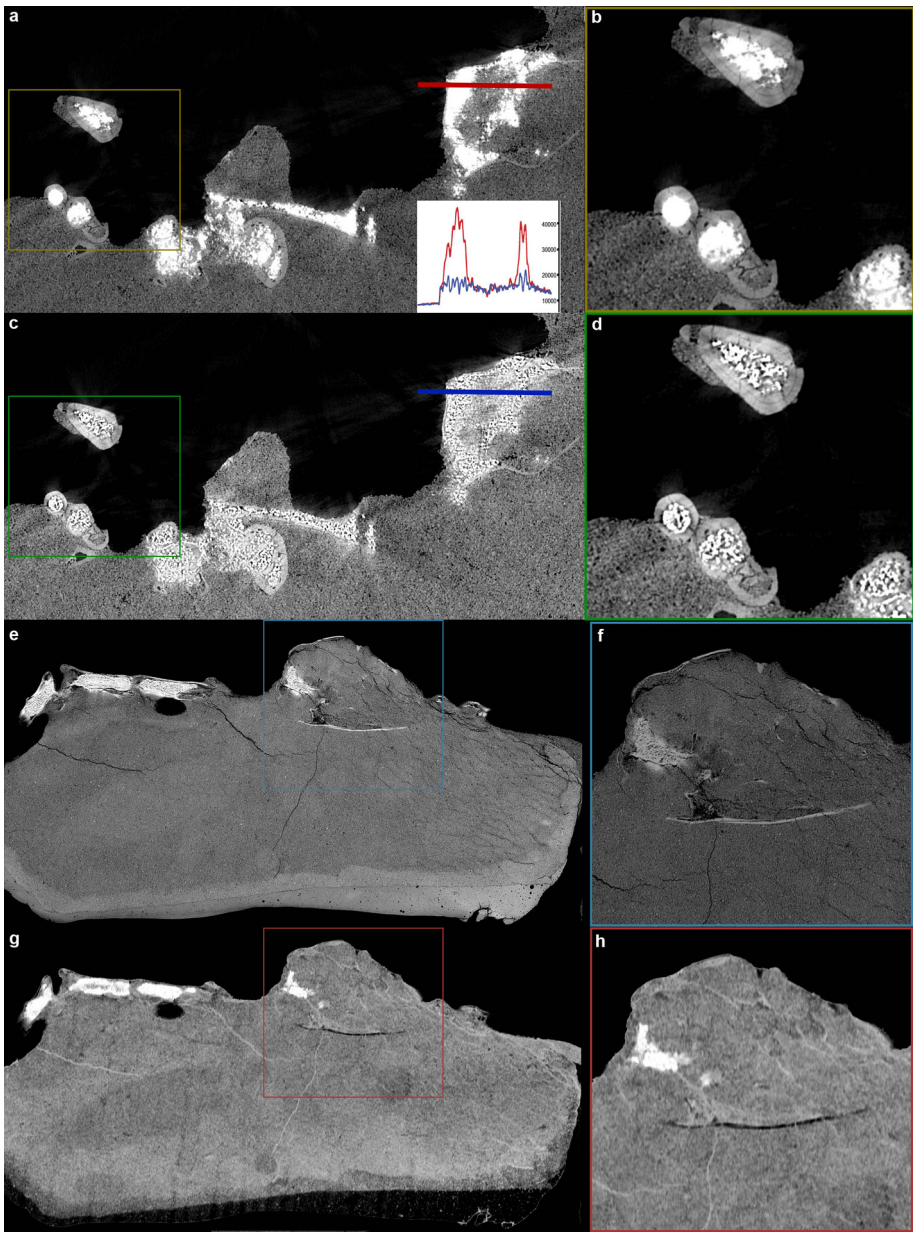

Extended Data Figure 1 | Example of data processed with texture enhancement and metallic-inclusion correction algorithms. a, Virtual section or the original dataset. **b**, Detail of **a**. **c**, Virtual section from the dataset corrected for metallic inclusions. **d**, Detail of **c**. Histograms along the blue and red lines demonstrate how metallic inclusions prevent adjusting the contrast to focus on the bone–matrix contact. **e**, Virtual section along the longitudinal axis of the cranium on dataset corrected for metallic inclusions. **f**, Detail of **e**. **g**, Same virtual section as in **e**, on data processed with the texture enhancement algorithm. **h**, Detail of **g**. In the processed data (**g**, **h**), homogenous parts (for example, bone or plaster) appear dark and the sediment reveals features that were barely visible prior to processing (**e**, **f**).

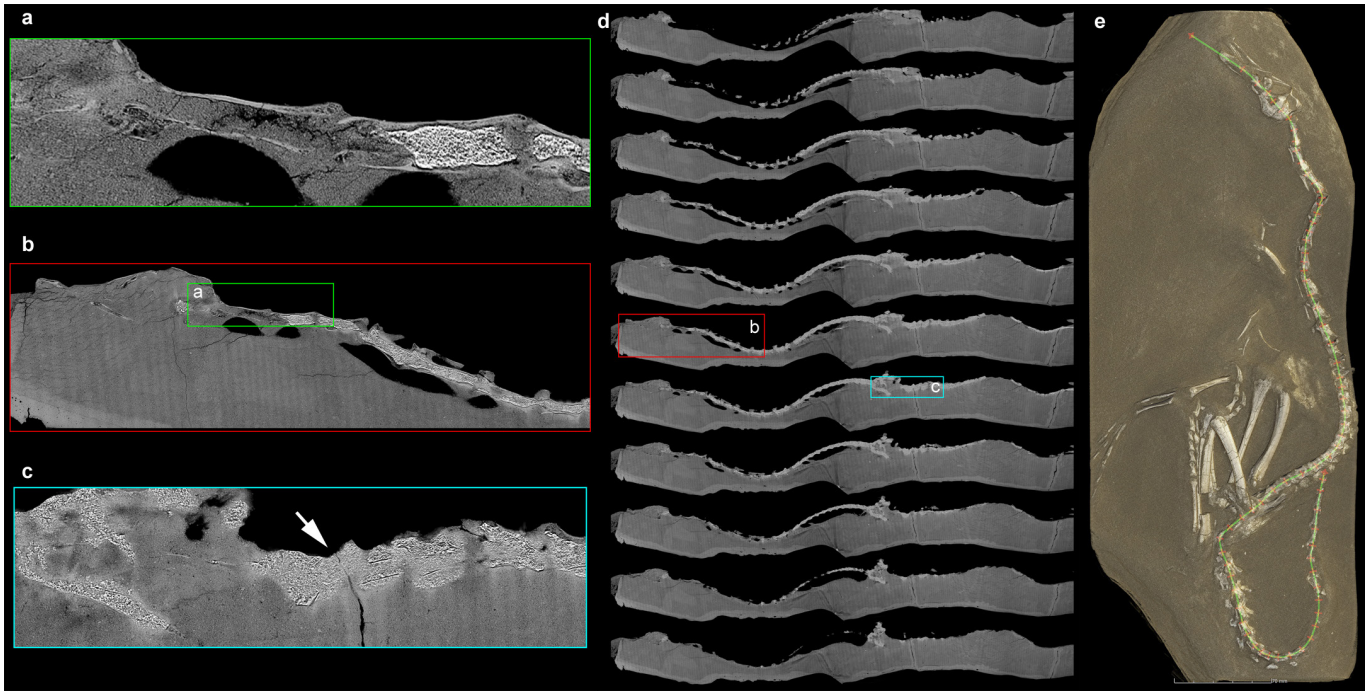

Extended Data Figure 2 | Sectional slices that illustrate the integrity of MPC-D102/109. a, Detail of anterior end of neck and posterior half of skull that shows continuity of the craniocervical transition. **b**, Detail of neck and skull that shows continuity between bones and matrix. **c**, Detail of proximal caudal series that shows the glued crack that crosses both matrix and bone (arrow), which confirms continuity between the sacrum and tail. **d**, Selected series of slices that show the continuity of bones and matrix along main slab. **e**, Overview of MPC-D102/109 indicating the curved virtual slice along a polyline (materialized above a 3D rendering) with slices at 5 mm on each side of this line every 1 mm. The line follows the axial column in order to show the continuity of the vertebral series. Scale bar, 70 mm. The renderings are generated using scan data that have been corrected for the absorbing metallic oxide infilling.

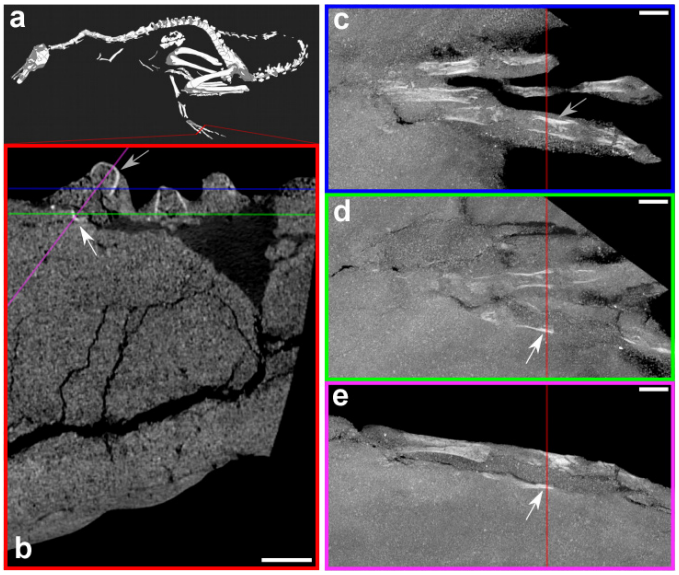

Extended Data Figure 3 | Cross-sectional slices that illustrate the integrity of the left manus in MPC-D102/109. a, Overview of MPC-D102/109 that indicates the location (red line) of the virtual sample for the slice shown in **b**. **b**, Dorsoventral cross-section of p2-I, p1-II and mc III; referred elements were stabilized close to their original position as indicated by the proximity of p2-I (grey arrow) to a small splint of p2-I that remained in the matrix (white arrow). Coloured lines indicate transects shown in **c** (blue), **d** (green) and **e** (purple). **c**, Mediolateral cross-section of manus with restored p2-I (grey arrow) indicated. **d**, Mediolateral cross-section of manus with *in situ* splint of p2-I (white arrow) indicated. **e**, Ventromedial–dorsolateral cross-section of manus with *in situ* splint of p2-I (white arrow) indicated. Scale bars, 20 mm. Sections in **b**–**e** were extracted from the dataset with an isotropic voxel size of 53.58 μm and volume reconstruction that followed a phase retrieval approach; **b** represents a single slice extracted from the digital volume and **c**–**e** were obtained through the thick-slab mode, with slab thickness set to 0.8 mm in 'Maximum' combine mode (VGStudio MAX 2.2.6, Volume Graphics).

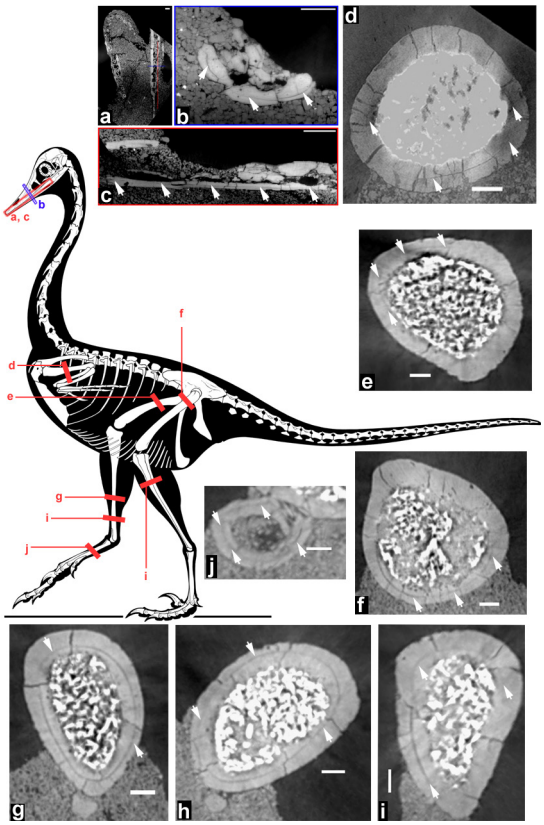

Extended Data Figure 4 | Cross-sectional slices reveal the consistent presence of a single line of arrested growth in the mandible and appendicular skeleton of MPC-D102/109. a, Longitudinal sections of skull (left) and left mandibular ramus (right) of MPC-D102/109 that indicate the locations of the virtual samples for slices shown in **b** (blue) and **c** (red). **b**, Transverse section of left mandibular ramus. **c**, Longitudinal cross-section of left mandibular ramus in dorsoventral plane. **d**, Cross-section of left humerus at mid-shaft. **e**, Cross-section of right femur shaft. **f**, Cross-section of left femur shaft. **g**, **h**, Cross-sections of right tibia distal shaft. **i**, Cross-section of left tibia proximal shaft. **j**, Cross-section of right metatarsal IV proximal shaft. White arrows indicate lines of arrested growth (LAGs). Scale bars, 2 mm (**a**–**c**), 0.8 mm (**d**), 1 mm (**e**–**h**) and 0.9 mm (**j**). Sections in **a**–**c** were extracted from the dataset with an isotropic voxel size of 2.25 μm, and volume reconstruction that followed a phase retrieval approach, as single slices in VGStudio MAX 2.2.6. The section in **d** was extracted from the dataset with an isotropic voxel size of 2.2 μm and volume reconstruction that followed a phase retrieval approach, and then recoded for improved contrast with the thick-slab mode set to 100 μm in the 'minimum' combine algorithm of VGStudio MAX 2.2.6. Sections in **e**–**j** were extracted from the dataset with an isotropic voxel size of 53.58 μm and volume reconstruction that followed a phase retrieval approach, with the thick-slab mode set to 100 μm in the 'minimum' combine algorithm of VGStudio 3.0.2.

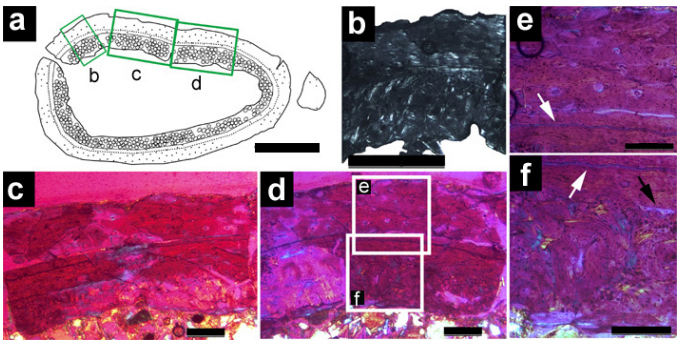

Extended Data Figure 5 | Histology of MPC-D102/109 left tibia and fibula. **a**, Interpretative histological drawing of tibia and fibula. **b**, Photomicrograph under cross-polarized light of boxed area in **a**. **c**, Cortical bone of the tibia under cross-polarized light with lambda waveplate, which reveals a LAG. **d**, Cortical bone of the tibia under cross-polarized light with lambda waveplate; this cross-section shows clearly the sharp cementing line boundary between the innermost remodelled and the outermost primary cortex. **e**, Close-up of the boxed area in **d**, with primary parallel-fibred bone with predominantly longitudinal canals and one LAG (white arrow) indicated. The cementing line that separates the outermost primary from the innermost remodelled cortex lies directly below the LAG. In the remodelled cortex, woven-bone osteocyte lacunae are visible in the lower left corner. No outer circumferential lamellae are visible. **f**, Close-up of the boxed area in **d**, with remodelled bone (black arrow) indicated. Several of the secondary osteons are surrounded by woven-bone osteocyte lacunae. A patch of inner circumferential lamellae is visible in the lower left corner. In panels **a** and **d**, **b**–**f** refer to their corresponding panels in the figure. Scale bars, 2 mm (**a**), 0.85 mm (**b**) and 0.35 mm (**c**–**f**).

Extended Data Figure 6 | 3D rendering of preantorbital part of the skull of MPC-D102/109. a, Dorsal view. **b**, Palatal view. p11, 11th premaxillary tooth; m16, 16th maxillary alveolus. **c**, Semi-transparent left lateral view that shows dentition. **d**, Left lateral view. af, antorbital fossa; en, external naris; mr, maxillary recess; pms, premaxillo-maxillary suture. **e**, Semi-transparent right lateral view that shows dentition. **f**, Right lateral view. en, external naris; nf, neurovascular foramina. Scale bars, 3 mm.

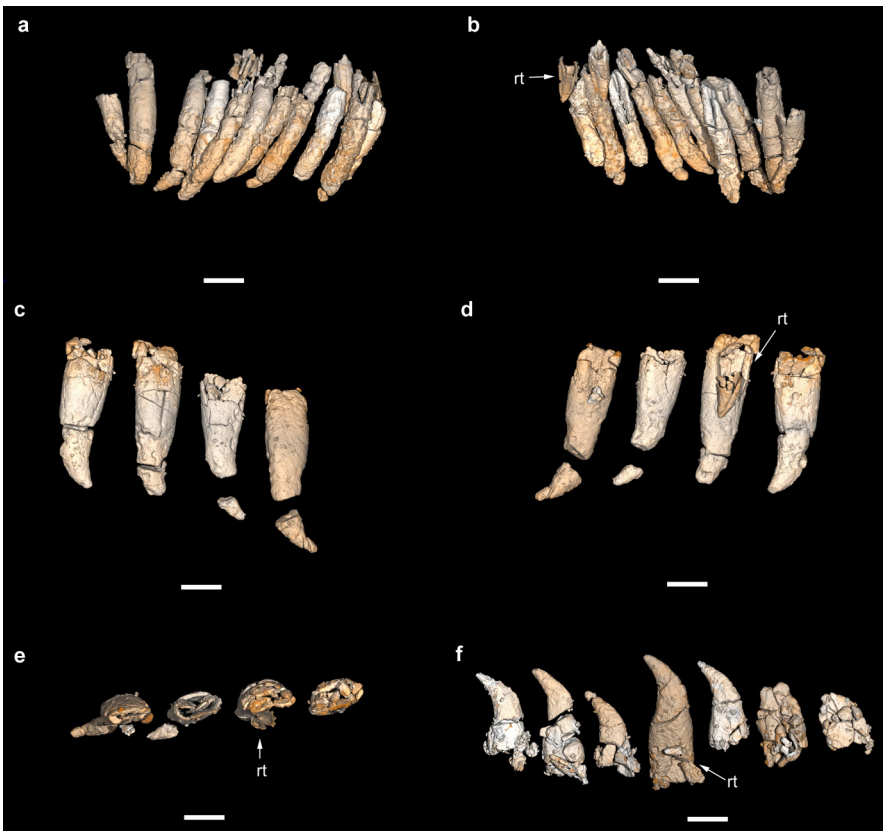

Extended Data Figure 7 | 3D rendering of dentition of MPC-D102/109. a, Premaxillary teeth in labial view. **b**, Premaxillary teeth in lingual view. **c**, Maxillary teeth in labial view. **d**, Maxillary teeth in lingual view. **e**, Maxillary teeth in basal view. **f**, Dentary teeth in lingual view. rt, replacement tooth. Scale bars, 1 mm.

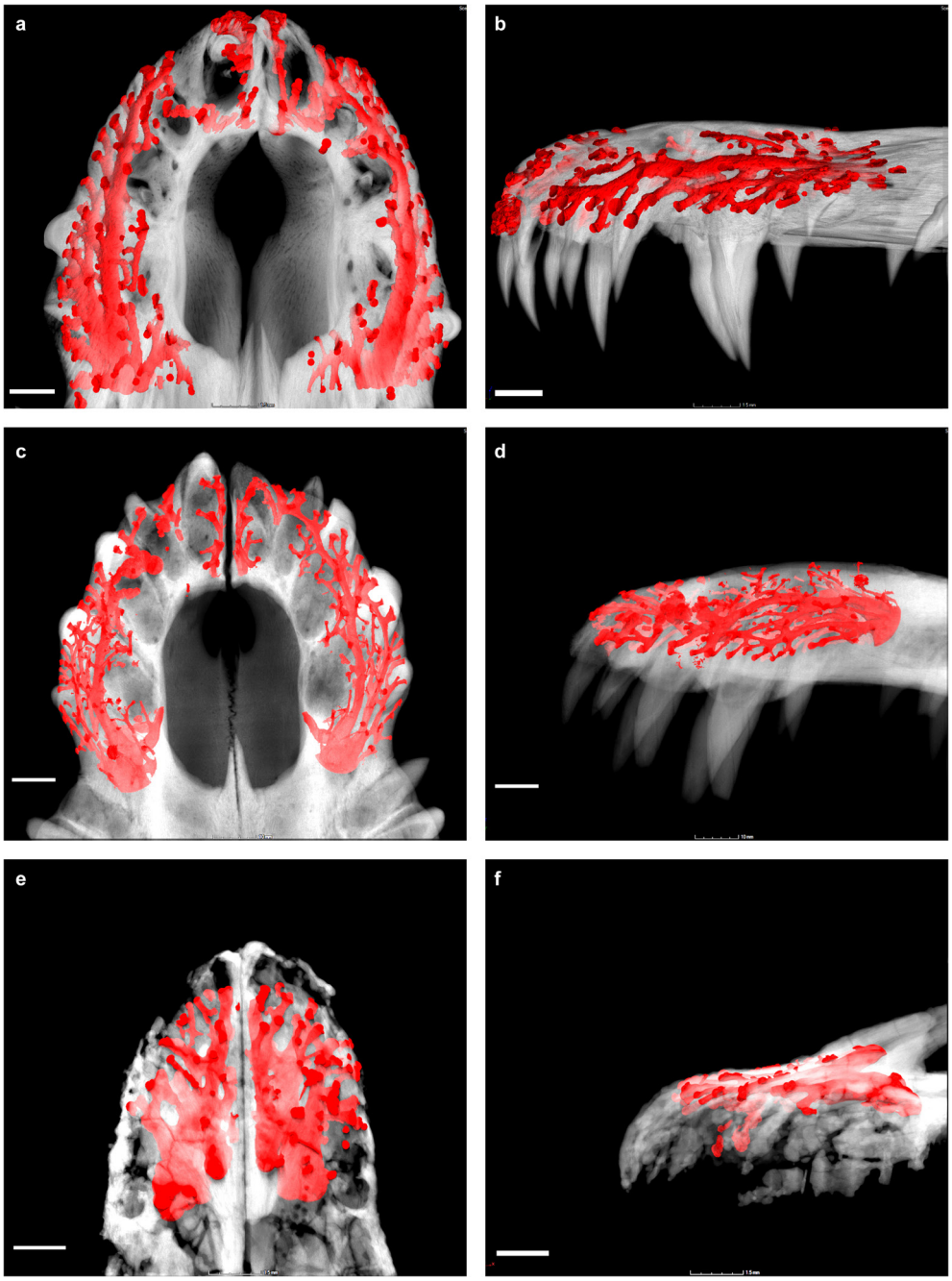

Extended Data Figure 8 | Comparison between synchrotron scan segmentations of the snouts of *Crocodylus niloticus* and *H. escuilliei*. **a**–**f**, Synchrotron scan segments that show the enlarged bony chambers that house the blood vessels and the rostral terminations of the maxillary branch of the trigeminal nerves (red) in the snouts of a two-year-old *C. niloticus* (**a**, **b**), a twenty-year-old *C. niloticus* (**c**, **d**) and *H. escuilliei* MPC-D102/109 (**e**, **f**). Dorsal (**a**, **c**, **e**) and lateral views (**b**, **d**, **f**) are shown. Scale bar, 1.5 mm (**a**, **b**, **e**, **f**), 10 mm (**c**, **d**).

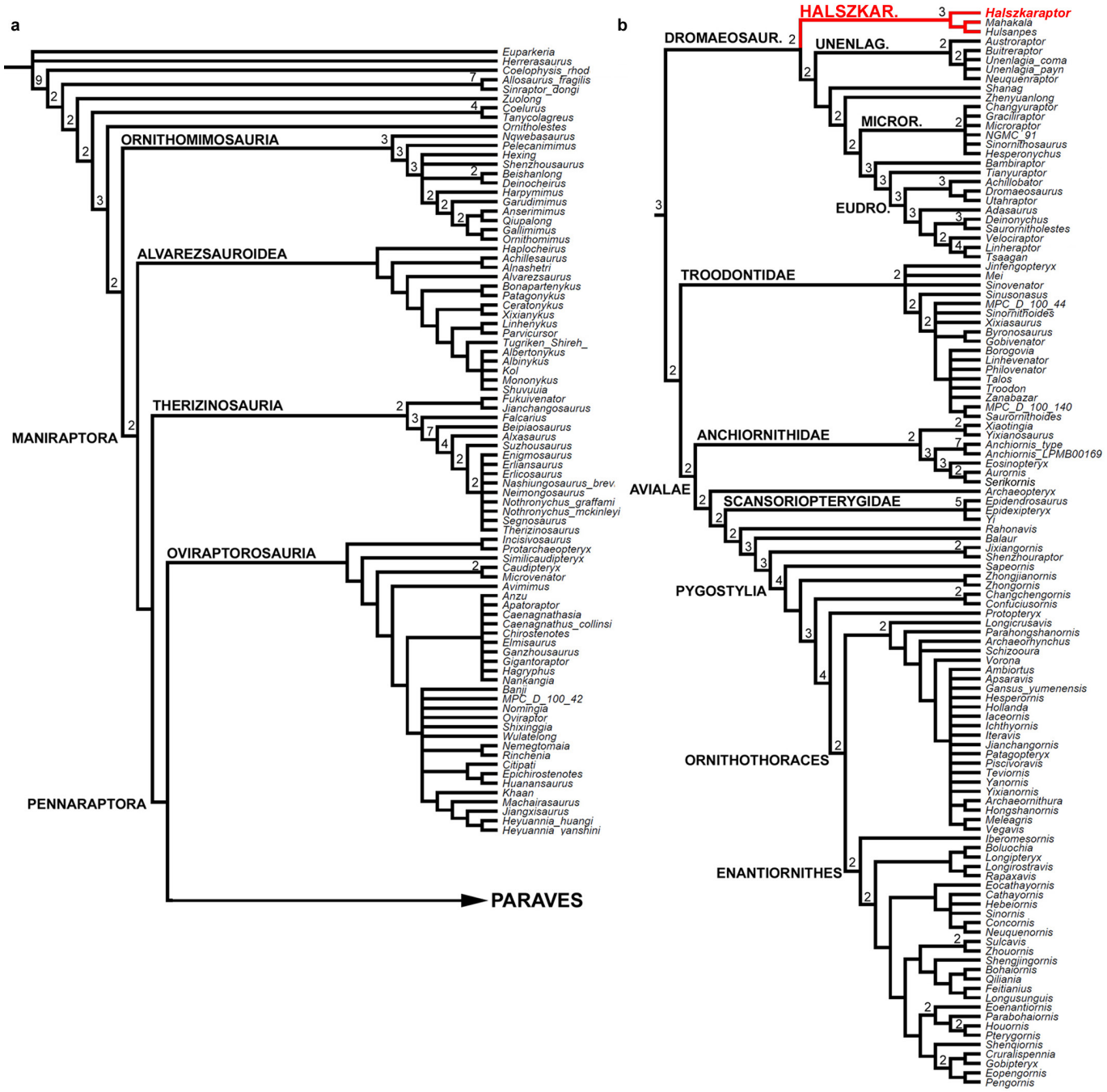

Extended Data Figure 9 | Strict consensus of the shortest trees found by the analysis of first dataset. a, Non-paravian taxa. **b**, Paraves. Numbers adjacent to nodes indicate decay index values >1 calculated when *Hulsanpes* and *Shanag* were pruned. DROMAEOSAUR., Dromaeosauridae; EUDRO., Eudromaeosauria; HALSZKAR., Halszkaraptorinae; MICROR., Microraptorinae; UNENLAG., Unenlagiinae.

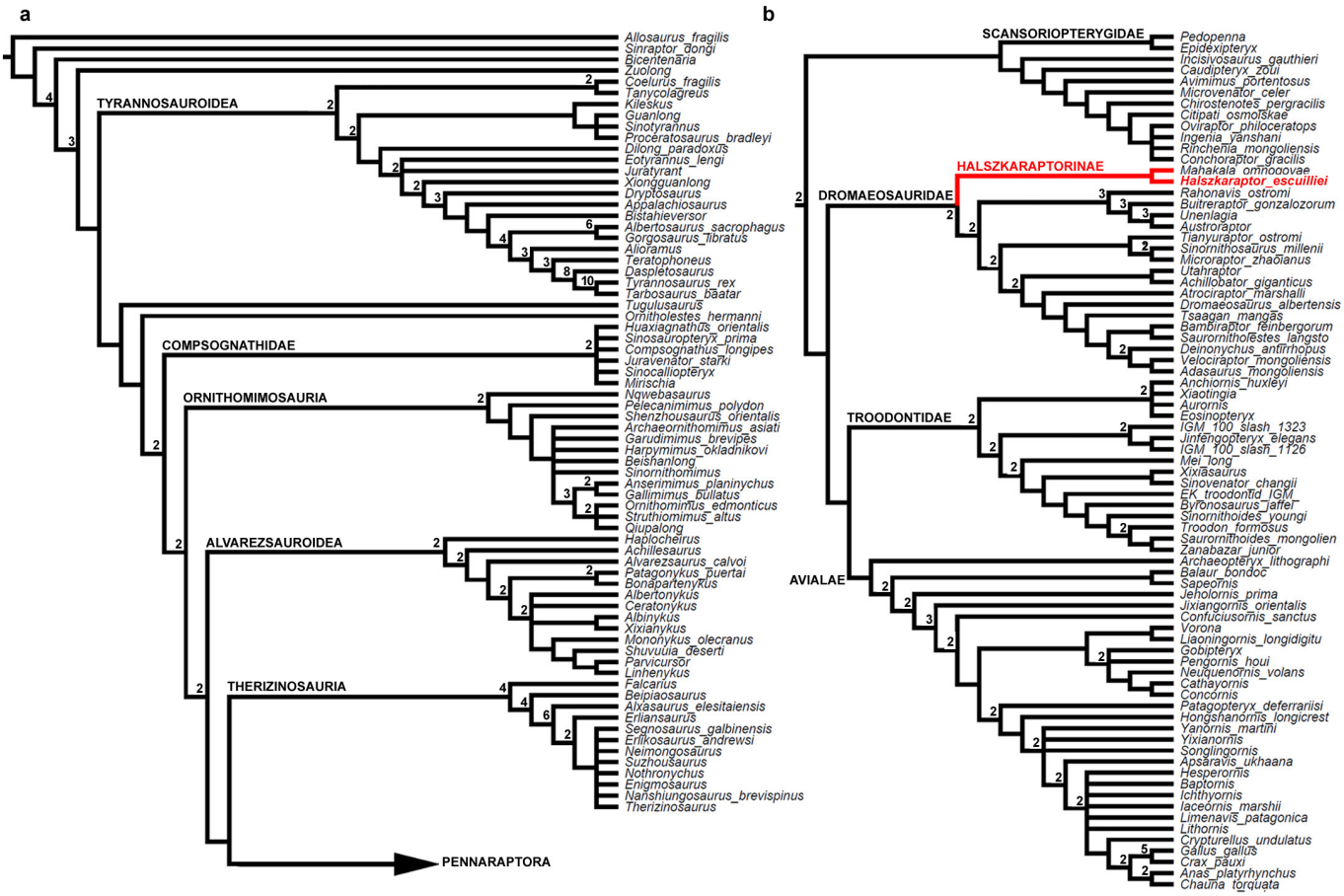

Extended Data Figure 10 | Reduced strict consensus of the shortest trees found by the analysis of the second dataset. a, Non-pennaraptoran taxa; **b**, Pennaraptora. Numbers adjacent to nodes indicate decay index values >1.

nature research

Corresponding author(s): Andrea CAU

☐ Initial submission ☐ Revised version ☒ Final submission

Life Sciences Reporting Summary

Nature Research wishes to improve the reproducibility of the work that we publish. This form is intended for publication with all accepted life science papers and provides structure for consistency and transparency in reporting. Every life science submission will use this form; some list items might not apply to an individual manuscript, but all fields must be completed for clarity.

For further information on the points included in this form, see Reporting Life Sciences Research. For further information on Nature Research policies, including our data availability policy, see Authors & Referees and the Editorial Policy Checklist.

Experimental design

1. Sample size

Describe how sample size was determined.

No sample size calculation was performed, as the majority of taxa are fossils with a very small sample size (often based on only a single individual known).
Sample size in morphometric data set 2 based on Hinić-Frlog & Motani (2010).

2. Data exclusions

Describe any data exclusions.

From morphometric data set 2, parameters not available in Halzkaraptor were excluded from analysis, in order to avoid a priori assumptions on missing data.

3. Replication

Describe whether the experimental findings were reliably reproduced.

For each morphometric data set, 1000 pseudo-replications of parameters were performed.

4. Randomization

Describe how samples/organisms/participants were allocated into experimental groups.

n/a

5. Blinding

Describe whether the investigators were blinded to group allocation during data collection and/or analysis.

n/a

Note: all studies involving animals and/or human research participants must disclose whether blinding and randomization were used.

6. Statistical parameters

For all figures and tables that use statistical methods, confirm that the following items are present in relevant figure legends (or in the Methods section if additional space is needed).

n/a	Confirmed	
☐	☒	The exact sample size (*n*) for each experimental group/condition, given as a discrete number and unit of measurement (animals, litters, cultures, etc.)
☒	☐	A description of how samples were collected, noting whether measurements were taken from distinct samples or whether the same sample was measured repeatedly
☐	☒	A statement indicating how many times each experiment was replicated
☒	☐	The statistical test(s) used and whether they are one- or two-sided (note: only common tests should be described solely by name; more complex techniques should be described in the Methods section)
☒	☐	A description of any assumptions or corrections, such as an adjustment for multiple comparisons
☒	☐	The test results (e.g. *P* values) given as exact values whenever possible and with confidence intervals noted
☒	☐	A clear description of statistics including central tendency (e.g. median, mean) and variation (e.g. standard deviation, interquartile range)
☒	☐	Clearly defined error bars

See the web collection on statistics for biologists for further resources and guidance.

Software

Policy information about availability of computer code

7. Software

Describe the software used to analyze the data in this study.	Phylogenetic data analyzed using TNT vers. 1.5. Morphometric data analyzed using PAST vers. 2.17c

For manuscripts utilizing custom algorithms or software that are central to the paper but not yet described in the published literature, software must be made available to editors and reviewers upon request. We strongly encourage code deposition in a community repository (e.g. GitHub). *Nature Methods* guidance for providing algorithms and software for publication provides further information on this topic.

Materials and reagents

Policy information about availability of materials

8. Materials availability

Indicate whether there are restrictions on availability of unique materials or if these materials are only available for distribution by a for-profit company.	n/a

9. Antibodies

Describe the antibodies used and how they were validated for use in the system under study (i.e. assay and species).	n/a

10. Eukaryotic cell lines

a. State the source of each eukaryotic cell line used.	n/a
b. Describe the method of cell line authentication used.	n/a
c. Report whether the cell lines were tested for mycoplasma contamination.	n/a
d. If any of the cell lines used are listed in the database of commonly misidentified cell lines maintained by ICLAC, provide a scientific rationale for their use.	n/a

Animals and human research participants

Policy information about studies involving animals; when reporting animal research, follow the ARRIVE guidelines

11. Description of research animals

Provide details on animals and/or animal-derived materials used in the study.	n/a

Policy information about studies involving human research participants

12. Description of human research participants

Describe the covariate-relevant population characteristics of the human research participants.	n/a